



Article

Thermal Analysis of Energy Storage Capacity According to Thickness of Nickel/Chromium Alloy Layer

Yonghyeon Kim ^{1,†}, Hyeokjoo Choi ^{2,†} , Seokhun Kwon ², Seokwon Lee ², Hyunil Kang ² and Wonseok Choi ^{2,*} 

¹ Department of Advanced Materials Engineering, Hanbat National University, Daejeon 34158, Korea; kjw4493@naver.com

² Department of Electrical Engineering, Hanbat National University, Daejeon 34158, Korea; hyukju1210@hanmail.net (H.C.); kwon1567@naver.com (S.K.); dltjrdnjs000@naver.com (S.L.); hikang@hanbat.ac.kr (H.K.)

* Correspondence: wschoi@hanbat.ac.kr

† Both authors contributed equally to this work.

Abstract: This paper examines a microconstruction consisting of nickel (Ni)/chromium (Cr) alloy thin-film. The total length of the microconstruction was 28 mm, the width was 0.2 mm, and the height was designed to be 1 μm . A thin-film of Ni/Cr alloy was co-sputtered on a silicon dioxide wafer patterned with photoresist via a RF magnetron sputtering system. The RF power ratios applied to the 4 inch target of Ni and Cr were 300 W:100 W (3:1), 300 W:150 W (2:1), and 150 W:150 W (1:1). The electrical resistance of the manufactured microconstruction was calculated and measured through Hall measurements. The temperature generated by applying 1–10 V to the microconstruction electrode was observed by using an infrared camera, and was summarized using a linear equation according to the power applied to each sample.



Citation: Kim, Y.; Choi, H.; Kwon, S.; Lee, S.; Kang, H.; Choi, W. Thermal Analysis of Energy Storage Capacity According to Thickness of Nickel/Chromium Alloy Layer. *Energies* **2021**, *14*, 3217. <https://doi.org/10.3390/en14113217>

Academic Editors: Ángel Galán Martín and Carlos Pozo

Received: 23 April 2021
Accepted: 24 May 2021
Published: 31 May 2021

Publisher's Note: MDPI stays neutral with regard to jurisdictional claims in published maps and institutional affiliations.



Copyright: © 2021 by the authors. Licensee MDPI, Basel, Switzerland. This article is an open access article distributed under the terms and conditions of the Creative Commons Attribution (CC BY) license (<https://creativecommons.org/licenses/by/4.0/>).

Keywords: co-sputtering; microconstruction; RF power; nickel/chromium alloy

1. Introduction

Device miniaturization through microfabrication leads to the development of new functions and performance [1–3]. Microconstruction, which is the aggregate of microfabrication, is frequently used in applications such as gas sensors, biosensors, micro explosive boiling, and flow rate sensors [4–8]. Acquiring the target temperature generated by a Joule heating-based microconstruction requires materials that have low resistivity, a low coefficient of thermal expansion, and homogenous temperature distribution [9–11]. Microconstructions of platinum (Pt) or gold (Au) are robust, stable and can provide a wide temperature range because they have a low coefficient of thermal expansion (Pt: 8.8 ppm/K, Au: 16.5 ppm/K) and resistivity (Pt: 10.9 $\mu\Omega\text{cm}$, Au: 2.40 $\mu\Omega\text{cm}$) [12–15]. However, these materials are too expensive to be used as targets for sputtering systems, which is an important part of the microfabrication process [16]. Nickel (Ni) and chromium (Cr) are relatively low-cost targets that could replace these metals. The Ni thin-film has lower resistivity (6.84 $\mu\Omega\text{cm}$) than Pt and a lower coefficient of thermal expansion than Au (Ni: 13 ppm/K) [15]. The Cr thin-film has higher resistivity (12.9 $\mu\Omega\text{cm}$) but a lower coefficient of thermal expansion (6 ppm/K) than Pt and Au [15]. A composite of these two materials, which both have good properties, Ni/Cr alloy thin-film, could have several useful resistivity and mechanical properties. A microconstruction based on Ni/Cr alloy thin-film by co-sputtering could be an excellent alternative to expensive Pt or Au.

In this paper, a microconstruction consisting of Ni/Cr alloy thin-film was fabricated. First, photoresist (PR) was applied as a meander-shaped pattern on a cleaned silicon dioxide (SiO_2) wafer. After that, Ni and Cr were co-sputtered on the PR-patterned SiO_2 wafer by applying different RF power. Ni/Cr alloy thin-films deposited on the PR were lifted-off in acetone solution. The surface properties of the fabricated Ni/Cr alloy thin-films were observed. The resistivity of the prepared samples was confirmed through Hall

measurements, and the calculated resistance was compared with the actual resistance. The heating characteristics were confirmed by applying 1–10 V to the microconstruction electrode and these were expressed as a linear regression equation.

2. Experiment

2.1. Microconstruction Design

Ni/Cr alloy, which is low-cost, stable, and robust, was selected as the electrode material for microconstruction. The microconstruction by Joule heating follows Equation (1).

$$P = V \cdot I \quad (1)$$

where V is the voltage applied to the microconstruction electrode, I is the current according to the voltage, and P is the heating power. The I changes according to the resistance (R) of the thin-film microconstruction and the V applied thereto. Therefore, by employing Ohm's Law, Equation (1) can be reorganized into Equation (2).

$$P = V \cdot I = V^2/R \quad (2)$$

From Equation (2), it can be inferred that the lower R , the higher P . Since R depends on the design of the microconstruction, the power consumption can be induced through the intentional R . The R of the thin-film microconstruction is as follows:

$$R = \rho L/wt \quad (3)$$

where ρ is the resistivity of the materials, and L , w and t are the total length, width, and thickness of the thin-film microconstruction, respectively. Several R -values can be obtained by adjusting these parameters. Figure 1 shows the structure of the patterned microconstruction used in this paper, and the designed L , w and t were 28 mm, 0.2 mm, and 1 μm , respectively.



Ni/Cr alloy based microconstruction

Figure 1. Schematic of meander-type Ni/Cr alloy-based microconstruction.

As shown in Figure 2, the ρ of the samples was observed through Hall measurements. When the RF power ratio applied to the 4 inch Ni and Cr targets was 3:1, 2:1, and 1:1, the ρ values were 247, 150, and 91 $\mu\Omega\text{cm}$, respectively. It was observed that ρ decreased as the RF power applied to the Cr target increased [17]. The R of the samples was obtained by substituting the designed L , t , and w in Figure 1 and the ρ values of each material in Figure 2 into Equation (3). The calculated R values are summarized in Table 1.

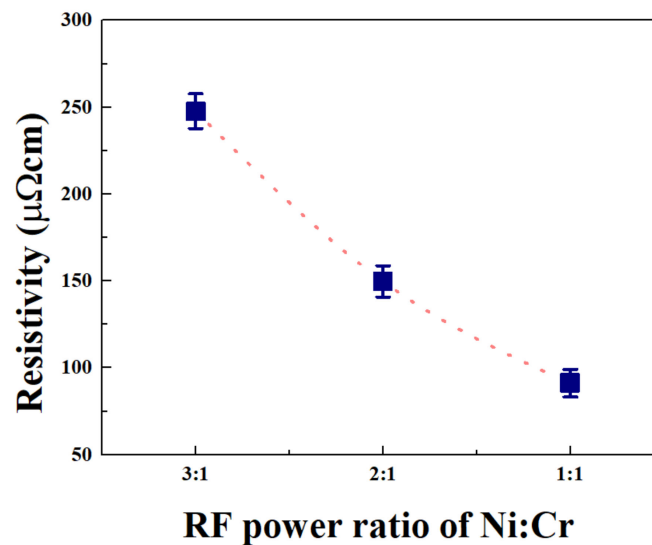


Figure 2. Resistivity of the samples via Hall measurement.

Table 1. Characteristics of the designed microconstruction.

RF Power Ratio (Ni:Cr)	L (mm)	w (mm)	t (μm)	ρ ($\mu\Omega\text{cm}$)	R (Ω)
3:1	28	0.2	1	247	346
2:1	28	0.2	1	150	210
1:1	28	0.2	1	91	127

2.2. Microconstruction Fabrication

The starting material, a 4 inch SiO_2 wafer (100, wet-3000 Å) was sonicated in the following order: trichloroethylene (purity of $\geq 99.5\%$), acetone (purity of $\geq 99.5\%$), methanol (purity of $\geq 99.8\%$), and deionized water ($\geq 18.2 \text{ M}\Omega\cdot\text{cm}$ @25 °C) for 10 min each. PR (AZ GXR-601 46cp) was patterned on the cleaned SiO_2 wafer through a photolithography process. The Ni/Cr alloy thin-film was deposited on the PR patterned wafer through a RF magnetron sputtering system. Table 2 shows the specific deposition conditions for the Ni/Cr alloy thin-film samples. All samples were deposited at room temperature with a working vacuum of 1.5×10^{-2} Torr by injecting 60 sccm of argon gas. The reason for the different deposition times is to obtain t of 1 μm . After the deposition of the Ni/Cr alloy thin-film was completed, the designed microconstruction was obtained through the lift-off process. Finally, polydimethylsiloxane (PDMS), which is used as a protective film, was spin-coated. Figure 3 shows the fabrication process of a Ni/Cr alloy thin-film based microconstruction.

Table 2. RF magnetron sputtering system conditions for co-sputtered Ni/Cr alloy thin-film.

Parameter	3:1 Sample	2:1 Sample	1:1 Sample
RF power (W)	300 W:100 W	300 W:150 W	150 W:150 W
Deposition time	38 min 20 s	22 min 30 s	50 min

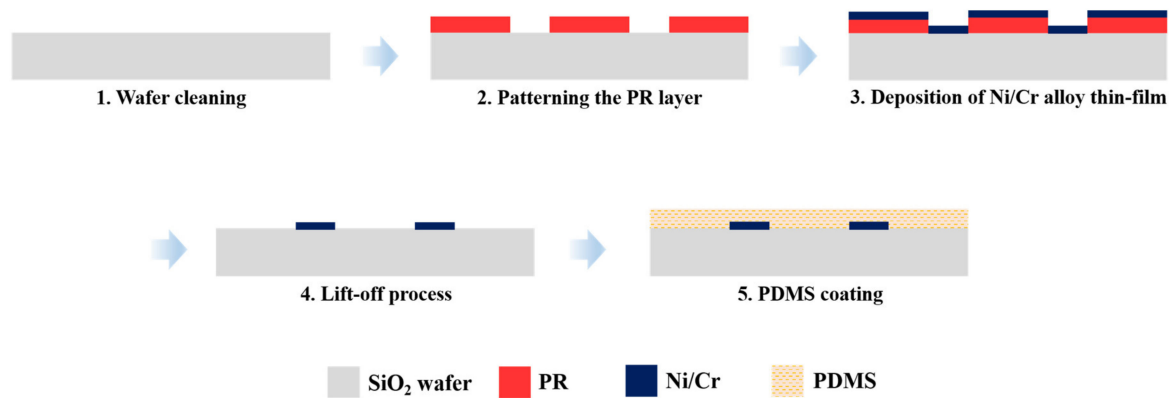


Figure 3. Process of Ni/Cr alloy thin-film-based microconstruction fabrication.

2.3. Characterization and Measurement

The prepared samples were cut into samples measuring $2 \times 2 \text{ cm}^2$. The surface characteristics of the manufactured microconstruction were observed through field emission scanning electron microscope (FESEM, HITACHI, S-4800) with a 10 kV accelerating voltage. The heating characteristics of the microconstruction were confirmed by applying 1–10 V as shown in Figure 4. The temperature according to the applied power was obtained through the infrared camera. The relationship between the heating temperature (y) and the applied power (x) was summarized. The ambient temperature was about $15 \text{ }^\circ\text{C}$ and the humidity was 70% during the measuring process.

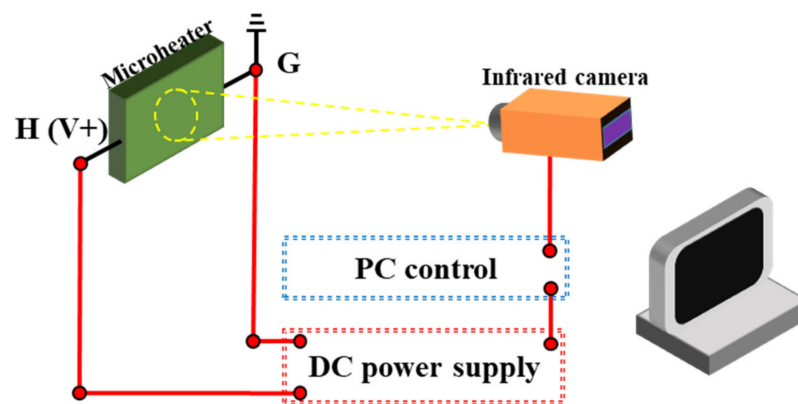


Figure 4. Schematic of microconstruction heating measurement.

3. Results and Discussion

3.1. Surface Characterization of Microconstruction

The FE-SEM cross-sectional image and EDS analysis were used to investigate the surface characteristics of the fabricated microconstruction with various components of Ni/Cr. Figure 5a shows the surface characteristics of the 3:1 sample. It was observed that the height of the 3:1 sample coincides with the thickness ($1 \text{ }\mu\text{m}$) required. The result of EDS analysis, independent of the determination of the RF power as 3:1, showed that the composition ratio of Ni and Cr atoms was close to 2:1 (Ni/Cr: 70.18 wt%/29.82 wt%; Ni/Cr: 67.58 at%/32.42 at%). Figure 5b displays the surface properties of the 2:1 sample. The height of the Ni/Cr thin-film in the 2:1 sample ($0.992 \text{ }\mu\text{m}$) differs from our desired height by about 8 nm, so, the measured actual resistance is $211.69 \text{ }\Omega$ with an error rate (Err) of 0.8%. According to the results of EDS analysis, its composition ratio was 57.4 wt% (54.4 at%) for Ni atoms and 42.6 wt% (45.6 at%) for Cr atoms. The 1:1 sample exhibits the largest Err (5%) because the measured thickness (t_{mea}) was about 950 nm and through the surface characteristics, as shown in Figure 5c. The composition ratio of Ni and Cr

atoms in the 1:1 sample was 1:2 (Ni/Cr: 33.36 wt%/66.64 wt%; Ni/Cr: 30.72 at%/69.28 at%). Overall, the thickness of the SiO₂ layer, which is under the Ni/Cr thin-film, was 300 nm. In addition, as the RF power applied to the Cr target increases compared to Ni, the composition ratio of Cr atoms in the sample increases. When the same RF power is applied to both targets (1:1 sample), the composition ratio of Cr atoms was higher. Table 3 summarizes the Err from the height difference between the designed microconstruction and the measured samples.

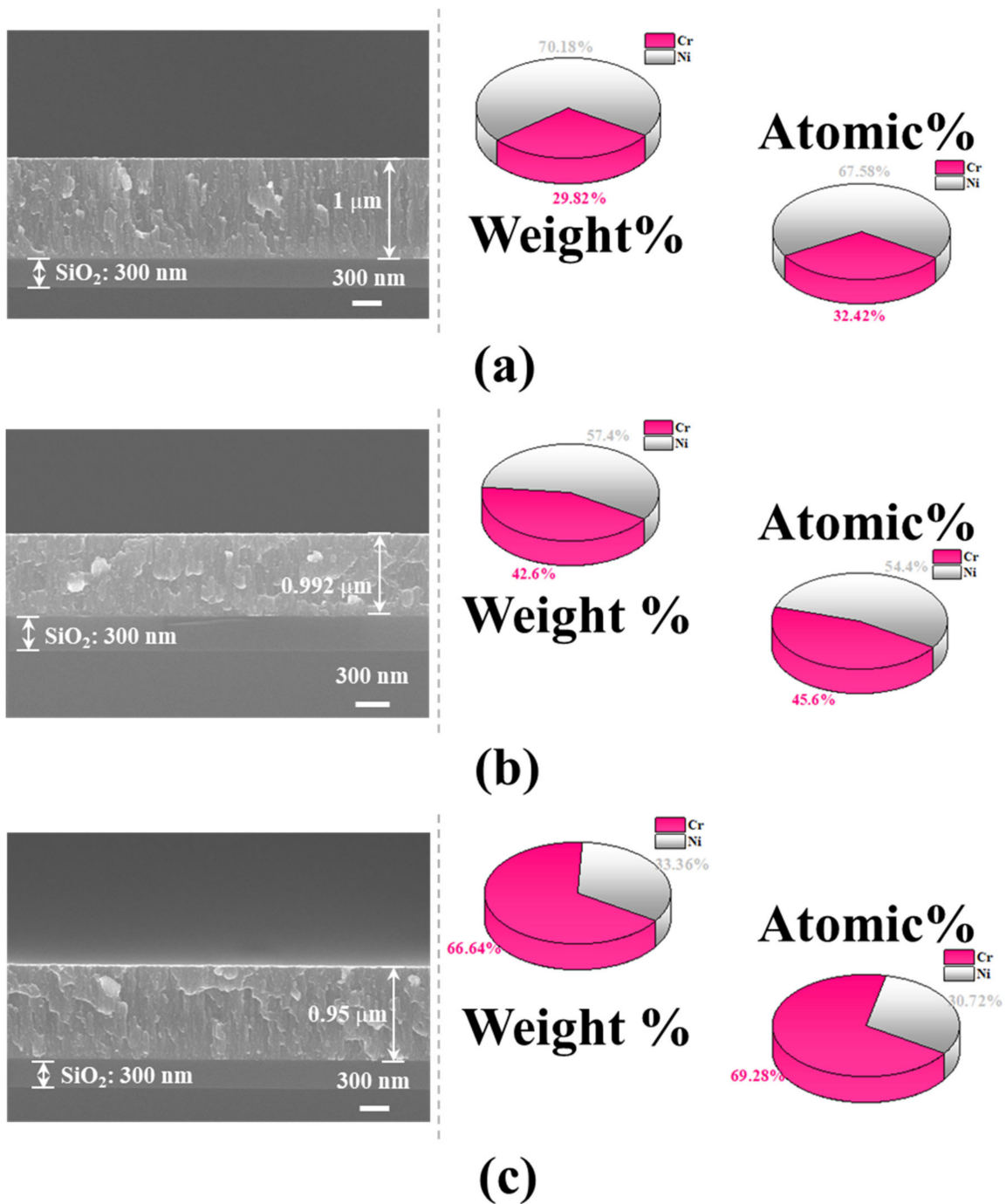


Figure 5. FE-SEM image (left) and EDS component analysis of the samples (right): (a) 3:1, (b) 2:1, and (c) 1:1.

Table 3. Characteristics of measured Ni/Cr alloy thin-film microconstruction.

RF Power Ratio (Ni:Cr)	t_{mea} (μm)	R_{req} (Ω)	R_{mea} (Ω)	Err (%)
3:1	1	346	346	0
2:1	0.992	210	211.69	0.8
1:1	0.95	127	133.68	5

3.2. Heating Characteristics of Microconstruction

The heating temperature in Joule heat-based microconstructions can be inferred according to the resistance of the material and the applied voltage. Figure 6 shows the heating characteristics of the samples. The heating characteristics of the 3:1 sample (Figure 6a) appear to have the highest heating temperature even though it has the lowest conductivity among the samples, as summarized by the following equation:

$$y \text{ (}^\circ\text{C)} = 0.1533x \text{ (mW)} + 23.39 \quad (4)$$

where y is the generated temperature ($^\circ\text{C}$) and x is the applied power (mW). When 10 V (289 mW) was applied to the microconstruction electrode, the obtained temperature was 67.4 $^\circ\text{C}$. Figure 6b displays the heating characteristics of the 2:1 sample. The infrared camera inset image shows that it is 50.3 $^\circ\text{C}$ at an applied voltage of 10 V (472.4 mW). The exothermic characteristics of the 2:1 sample is as follows:

$$y \text{ (}^\circ\text{C)} = 0.0544x \text{ (mW)} + 25.185 \quad (5)$$

Figure 6c shows the heating characteristics of a 1:1 sample, which was 53.4 $^\circ\text{C}$ when the applied voltage was 10 V. The heating characteristics of a 1:1 sample can be summarized in the following equation:

$$y \text{ (}^\circ\text{C)} = 0.0444x \text{ (mW)} + 18.781 \quad (6)$$

All samples had a linear temperature according to the applied power, and the accuracy of linear regression lines (Equations (4)–(6)) was high because the coefficient of determination (R^2) was distributed in the range of 0.993 to 0.999. In addition, the slope of the linear regression was reduced as the ratio of Cr in the Ni/Cr alloy thin-film microconstruction increased.

We redesigned the 3:1 sample to fabricate a microconstruction with a resistance of 100 Ω . Figure 7 shows the actual image of the manufactured microconstruction and the infrared camera image of the temperature (171.3 $^\circ\text{C}$) when 10 V was applied. The manufactured microconstruction was designed with total length of l , thickness of t , and width of W . The actual resistance of the microconstruction measured with a multimeter was 103.63 Ω . When the measured resistance was substituted in Equations (2) and (4), the temperature was 171.2 $^\circ\text{C}$. Therefore, there was no significant difference between the measured and calculated temperature. It is expected that the desired target temperature can be obtained by designing the RF and applied power because of the high R^2 of the samples. Kang et al. reported that the electrical resistances of a Pt-based microconstruction were 127 and 171 Ω at 25 $^\circ\text{C}$ and 150 $^\circ\text{C}$ in the temperature oven, respectively [13]. Compared to Pt-based microconstruction, nickel–chromium alloy-based microconstruction have lower resistance and higher temperatures were confirmed. Therefore, it is more advantageous to use a cheaper nickel–chromium alloy-based microconstruction to achieve a higher temperature.

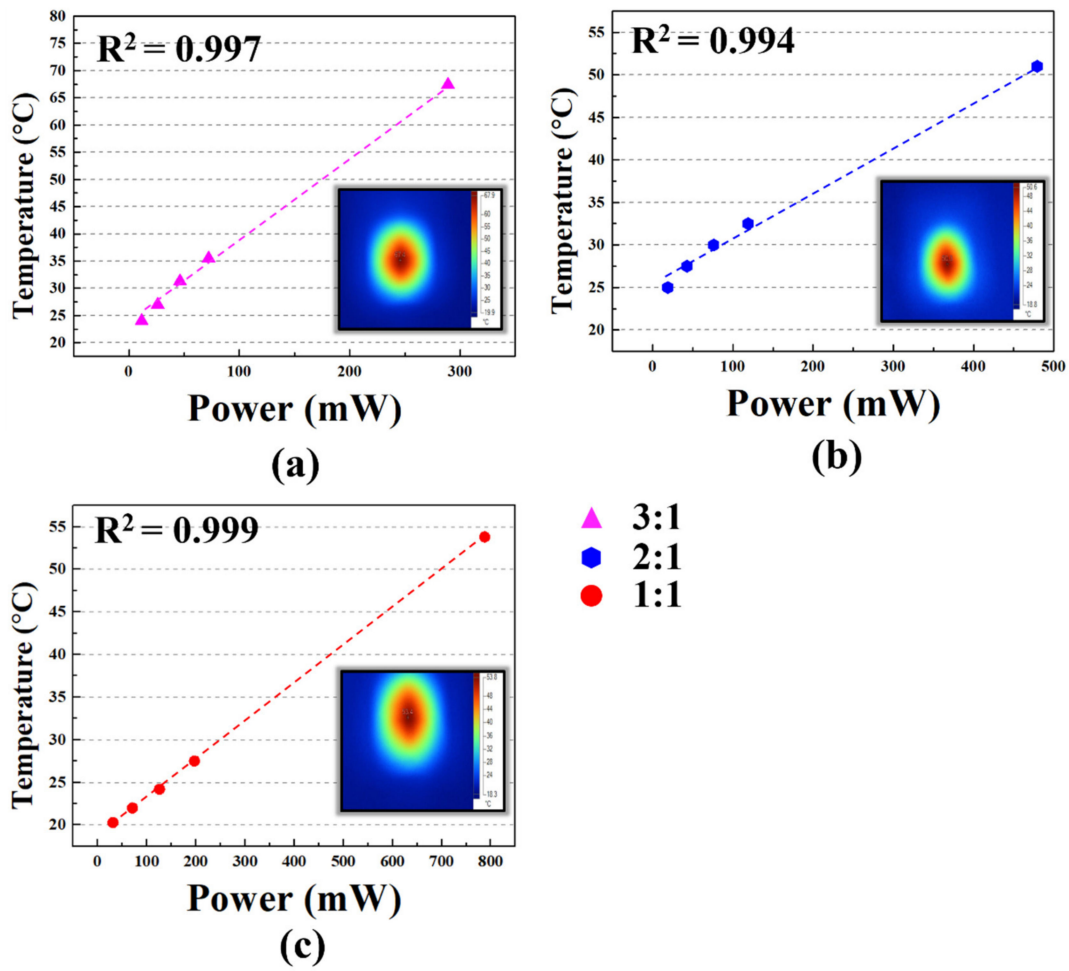


Figure 6. Temperature of microconstruction according to the applied power and infrared camera inset image when applying 10 V to the samples: (a) 3:1, (b) 2:1, and (c) 1:1.

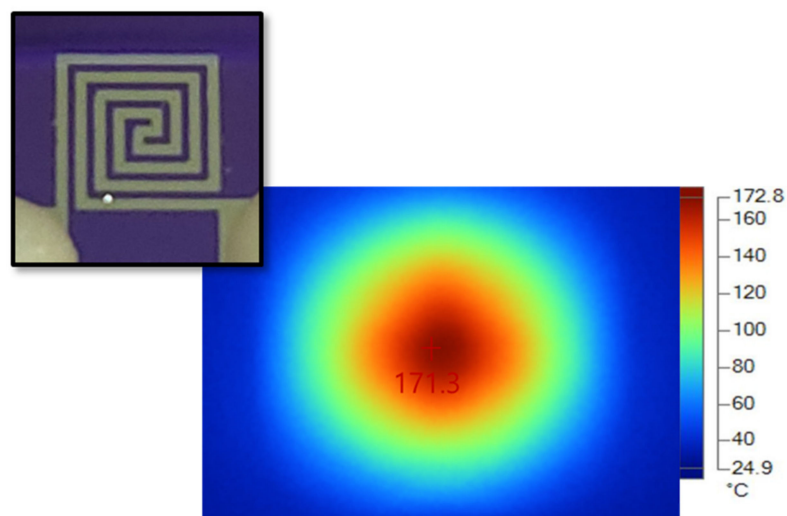


Figure 7. The image (left) and infrared camera image (right) of applying 10 V to a microconstruction redesigned for generating high temperatures.

4. Conclusions

Pt and Au are high-cost materials that are used as targets for sputtering systems, which are important in microfabrication processes. We studied whether Ni and Cr could be used as alternative targets to lower the costs. In order to fabricate the Joule heat-based microconstruction, thin-film composed of Ni/Cr alloy was co-sputtered on a SiO₂ wafer via a RF magnetron sputtering system. The ratio (Ni:Cr) of RF power applied to both targets was 3:1, 2:1, and 1:1. As a result of co-sputtering, it was observed through EDS analysis that when the same RF power was applied, more Cr atoms were deposited than Ni atoms. In addition, electrical conductivity improved as the RF power applied to the Cr target increased, compared to the Ni target. However, the 3:1 sample, which had the lowest electrical conductivity, had the best heat generation characteristics. The 3:1 sample was redesigned to generate high temperatures (171.3 °C) when 10 V was applied. Surprisingly, the desired temperature was achieved with the designed resistance due to the high accuracy of the linear regression equation. The co-sputtered Ni/Cr alloy thin-film microconstruction fabricated through a RF magnetron sputtering system can be designed to achieve target temperatures. Ni/Cr alloy thin-film manufactured through co-sputtering could be an excellent replacement for expensive Pt or Au.

Author Contributions: Conceptualization, Methodology, Writing—Original Draft, Data Curation H.C. and Y.K.; Writing—Review & Editing, Visualization, Data Curation, S.K.; Visualization, Data Curation, S.L.; Validation, Resources, H.K.; Writing—Review & Editing, Supervision, W.C. All authors have read and agreed to the published version of the manuscript.

Funding: This research was supported by the Korea Institute of Energy Technology Evaluation and Planning (KETEP), Ministry of Trade, Industry & Energy (MOTIE) of the Republic of Korea (No. 20204030200080) and Korea Electric Power Corporation (Grant number: R17XA05-01).

Institutional Review Board Statement: Not applicable.

Informed Consent Statement: Not applicable.

Data Availability Statement: No new data were created or analyzed in this study. Data sharing is not applicable to this article.

Conflicts of Interest: The authors declare no conflict of interest.

References

1. Chang, W.-Y.; Hsihe, Y.-S. Multilayer microheater based on glass substrate using MEMS technology. *Microelectron. Eng.* **2016**, *149*, 25–30. [[CrossRef](#)]
2. Wang, C.-P.; Hsiao, M.-H.; Lee, G.-H.; Chang, T.-L.; Lee, Y.-W. The investigation of electrothermal response and reliability of flexible graphene micro-heaters. *Microelectron. Eng.* **2020**, *228*, 111334. [[CrossRef](#)]
3. Kwon, J.Y.; Hong, S.J.; Kim, G.H.; Suh, Y.D.; Lee, H.B.; Choo, S.Y.; Lee, D.H.; Kong, H.J.; Yeo, J.Y.; Ko, S.H. Digitally patterned resistive micro heater as a platform for zinc oxide nanowire based micro sensor. *Appl. Surf. Sci.* **2018**, *447*, 1–7. [[CrossRef](#)]
4. Moalaghi, M.; Ghareh, M.; Ranjkesh, A.; Hossein-Babaei, F. Tin oxide gas sensor on tin oxide microheater for high-temperature methane sensing. *Mater. Lett.* **2020**, *263*, 127196. [[CrossRef](#)]
5. Castagna, M.E.; Petralia, S.; Amore, M.G.; Cappello, E.; Beninato, A.; Sinatra, V.; Baglio, S.; Conoci, S. A novel silicon based mags-biosensor for nucleic acid detection by magnetoelectronic transduction. *Sens. Bio Sens. Res.* **2015**, *6*, 85–89. [[CrossRef](#)]
6. Long, H.; Turner, S.; Yan, A.; Xu, H.; Jang, M.; Carraro, C.; Maboudian, R.; Zettl, A. Plasma assisted formation of 3D highly porous nanostructured metal oxide network on microheater platform for Low power gas sensing. *Sensors Actuators B Chem.* **2019**, *301*, 127067. [[CrossRef](#)]
7. Zhao, Z.; Glod, S.; Poulidakos, D. Pressure and power generation during explosive vaporization on a thin-film microheater. *Int. J. Heat Mass Transf.* **2000**, *43*, 281–296. [[CrossRef](#)]
8. Mavraki, E.; Moschou, D.; Kokkoris, G.; Vourdas, N.; Chatzandroulis, S.; Tserepi, A. A continuous flow μ PCR device with integrated microheaters on a flexible polyimide substrate. *Procedia Eng.* **2011**, *25*, 1245–1248. [[CrossRef](#)]
9. Roy, A.; Ender, F.; Azadmehr, M.; Aasmundtveit, K.E. CMOS micro-heater design for direct integration of carbon nanotubes. *Microelectron. Reliab.* **2017**, *79*, 517–525. [[CrossRef](#)]
10. Yu, S.; Wang, S.; Lu, M.; Zuo, L. A novel polyimide based micro heater with high temperature uniformity. *Sensors Actuators A Phys.* **2017**, *257*, 58–64. [[CrossRef](#)]
11. Ueno, R.; Kim, B. Reliable transfer technique of gold micro heater through different affinities of thiol (SH) and amine (NH₂) groups. *Microelectron. Eng.* **2017**, *171*, 6–10. [[CrossRef](#)]

12. Sharma, R.; Khanna, P. Lead free packaging of Pt micro-heater for high temperature gas sensors. *Fuel* **2013**, *112*, 550–556. [[CrossRef](#)]
13. Kang, J.-G.; Park, J.-S.; Shin, J.; Lee, E.-A.; Noh, S. Temperature control of micro heater using Pt thin film temperature sensor embedded in micro gas sensor. *Micro Nano Syst. Lett.* **2017**, *5*, 1–5. [[CrossRef](#)]
14. Son, J.M.; Lee, J.H.; Kim, J.; Cho, Y.H. Temperature distribution measurement of Au micro-heater in microfluidic channel using IR microscope. *Int. J. Precis. Eng. Manuf.* **2015**, *16*, 367–372. [[CrossRef](#)]
15. Liu, C. Thermal Bimorph Principle. In *Foundations of MEMS*; Gilfillan, A., Ed.; Pearson Education Limited: London, UK, 2011; pp. 198–205.
16. Matsuyama, K.; Tsubaki, T.; Kato, T.; Okuyama, T.; Muto, H. Preparation of catalytically active Au nanoparticles by sputter deposition and their encapsulation in metal-organic framework of $\text{Cu}_3(\text{BTC})_2$. *Mater. Lett.* **2020**, *261*, 127124. [[CrossRef](#)]
17. Petley, V.; Sathishkumar, S.; Raman, K.T.; Rao, G.; Chandrasekhar, U. Microstructural and mechanical characteristics of Ni–Cr thin films. *Mater. Res. Bull.* **2015**, *66*, 59–64. [[CrossRef](#)]